Letter | Editors' Suggestion

Quantum pathways of carrier and coherent phonon excitation in bismuth

Azize Koç,[1] Isabel Gonzalez-Vallejo,[1] Matthias Runge,[1] Ahmed Ghalgaoui,[1] Klaus Reimann,[1] Laurenz Kremeyer,[2,*] Fabian Thiemann,[2] Michael Horn-von Hoegen,[2] Klaus Sokolowski-Tinten,[2] Michael Woerner,[1,†] and Thomas Elsaesser[1]

[1]*Max Born Institute for Nonlinear Optics and Short Pulse Spectroscopy, Max-Born-Straße 2A, 12489 Berlin, Germany*

[2]*Department of Physics and Center for Nanointegration CENIDE, University of Duisburg-Essen, Lotharstraße 1, 47057 Duisburg, Germany*

(Received 29 July 2022; revised 20 October 2022; accepted 9 May 2023; published 23 May 2023)

Quantum pathways inducing coherent lattice dynamics are studied in bismuth (Bi). A crystalline Bi film is excited by femtosecond midinfrared pulses and transient intensity changes on the (111) Bragg reflection are probed by hard x-ray pulses. A fast decrease and coherent oscillations of the diffracted intensity display up to 50% and 10% intensity change, respectively. The oscillation frequency of 2.6 THz is independent of pump intensity. Midinfrared excitation opens different quantum pathways for electron-hole generation, such as field-driven carrier tunneling at the L points, which reduces the crystal symmetry and leads to optical phonon excitation at the X point with the strongest electron-phonon coupling.

DOI: 10.1103/PhysRevB.107.L180303

The coupling of electrons and holes to optical phonons is a basic interaction in crystalline solids, which determines electronic properties and induces nonequilibrium lattice dynamics. Ultrafast spectroscopy and structure research have provided insight in the excitation mechanisms of optical phonons, their role in carrier relaxation, and coherent lattice motions, connected to a periodic displacement of atoms from their equilibrium positions. In this context, the semimetal bismuth (Bi) is a prototypical system in which coherent optical phonon wave packets have been studied extensively in femtosecond all-optical and optical-pump/x-ray-diffraction-probe experiments. The latter are mapping lattice dynamics in space and time and thus give direct access to the time dependence of atomic displacements [1–6].

Coherent phonon dynamics of crystalline Bi, which belongs to the space group $R\bar{3}m$ with a threefold rotoinversion axis perpendicular to the (111) plane, has mostly been studied after interband excitation by femtosecond pulses centered at $\lambda_{ex} = 0.8$ μm [1–11]. The pump pulse generates electron-hole pairs via interband transitions at various points in k space. Upon excitation, the minimum of the potential energy surface of optical phonons is displaced along the phonon coordinate and a nonstationary superposition of phonon quantum states, i.e., a wave packet, is generated. In ultrafast x-ray diffraction measurements, a fast decrease and a periodic modulation of diffracted intensity on the (111) Bragg reflection have been observed [1–4].

For moderate excitation fluences $F \leqslant 1$ mJ/cm^2 at $\lambda_{ex} = 0.8$ μm, one detects oscillations with frequencies around $\nu = 2.5$ THz [Fig. 1(a)]. They are assigned to a wave-packet motion along the longitudinal A_{1g} phonon coordinate. With increasing pump fluence, the frequency of the oscillations decreases, reaching a value $\nu = 1.5$ THz around F=2.7 mJ/cm^2 [6]. This strong frequency reduction has been assigned to a softening of the interatomic A_{1g} phonon potential at high carrier densities [2].

The symmetry of the excited Bi lattice determines which phonons are excited displacively. In case the equilibrium $R\bar{3}m$ symmetry is preserved and the pump-probe measurement remains in the third-order ($\chi^{(3)}$) limit of light-matter interaction, only the A_{1g} phonon is excited. This condition may not be fulfilled in some of the experiments with excitation at $\lambda_{ex} = 0.8$ μm, in particular at high pump fluences. Femtosecond excitation with linearly polarized pulses at $\lambda_{ex} = 0.8$ μm initially generates an anisotropic multicomponent carrier distribution with a symmetry clearly different from equilibrium. As a result, also other optical phonons, e.g., of E_g symmetry, can be excited displacively. The initial carrier distribution transforms into a quasiequilibrium distribution of electrons and holes on a timescale of some 600 fs [12]. The transient crystal symmetry during carrier relaxation is not known and, in particular, the impact of carrier relaxation on the rise time of x-ray diffraction transients is not understood. As a result, the quantum pathways behind displacive phonon excitation are mainly unknown.

Excitation at wavelengths close to the direct energy gaps of Bi at the T points ($E_G^T = 350$ meV, $\lambda = 3.5$ μm) or the L points ($E_G^L = 15$ meV, $\lambda = 83$ μm) [13] avoids such complexity and holds potential for much more specific insight in the phonon driving mechanism. Moreover, the much larger penetration depth of midinfrared light in a Bi film allows for matching the excitation and the x-ray probing depth.

In this Letter, we present a femtosecond x-ray diffraction study of Bi with midinfrared excitation at $\lambda_{ex} = 5.0$ and 2.5 μm. On the (111) Bragg reflection, we observe a fast decrease and oscillatory intensity changes of large amplitude. The signal rises within the 150-fs time resolution of the ex-

*Present address: Department of Physics, Center for the Physics of Materials, McGill University, Montreal, Canada.

†woerner@mbi-berlin.de

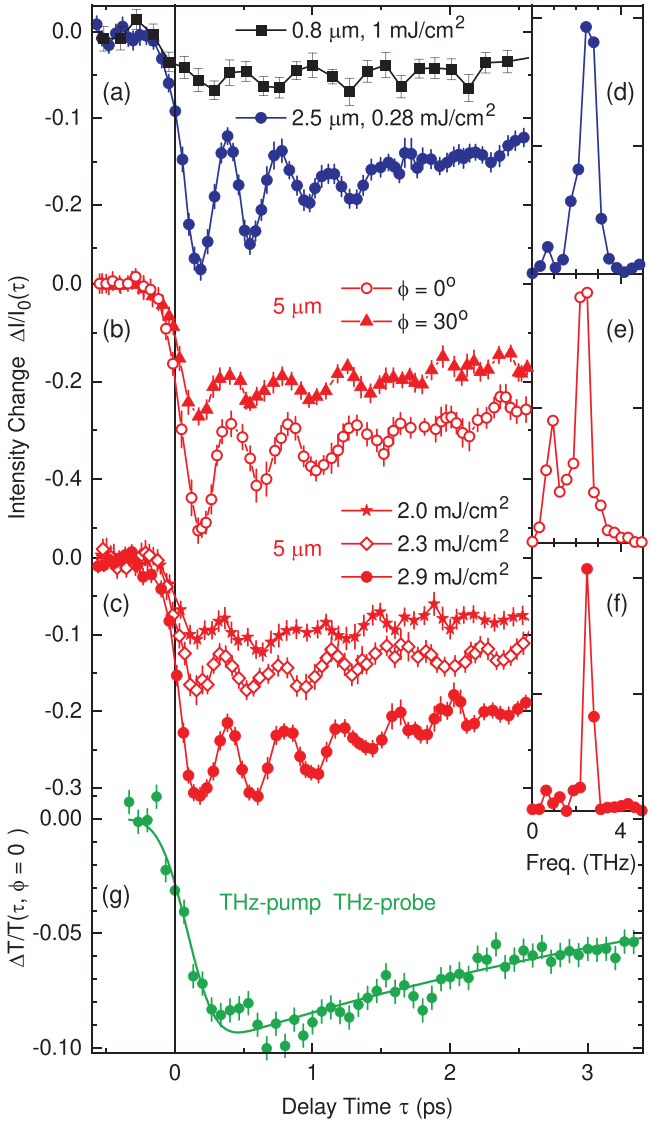

FIG. 1. (a)–(c) Transient intensity changes of the (111) Bragg reflection after excitation with femtosecond midinfrared pulses (red: $\lambda_{ex} = 5$ μm; blue: $\lambda_{ex} = 2.5$ μm; black: $\lambda_{ex} = 0.8$ μm). (b) Variation of the signal with azimuthal angle ϕ at a pump fluence of 2.6 mJ/cm^2, maximal signal at 0°, and minimal signal at 30°. (c) Transients for different pump fluences at $\phi = 15°$. (d)–(f) Fourier transforms of one signal each from (a)–(c). (g) THz-pump–THz-probe signal. The dots are the experimental results, and the solid line is a single-exponential fit.

periment, while phonon softening with increasing fluence is absent. We identify field-driven carrier tunneling at the L points as a quantum pathway of electron-hole and coherent phonon generation. This process reduces the crystal symmetry and allows, in turn, for displacive phonon excitation at the X point. This picture is supported by complementary THz experiments and band structure calculations.

In the femtosecond optical-pump/x-ray-diffraction-probe experiments, a single-crystal Bi film of 45 nm thickness is studied. The sample consists of a (111)-oriented Bi layer epitaxially grown on a (111)-oriented Si substrate [14]. The sample is excited by p-polarized midinfrared pulses at central wavelengths $\lambda_{ex} = 5$ or 2.5 μm and a duration of 80 fs under an incident angle of 68°. The relative intensity change of the (111) diffraction peak is monitored in reflection geometry by a hard x-ray probe pulse. The diffracted x-ray intensity is recorded with an area detector (EigerX-1M, Dectris) for pump-probe delays up to 5 ps.

An optical parametric chirped-pulse amplifier (OPCPA) with a 1 kHz repetition rate provides 80-fs pulses at a central wavelength of 5 μm with a pulse energy of 3 mJ [15]. A 2% fraction of the OPCPA output reflected from a beam splitter serves as a pump pulse at $\lambda_{ex} = 5$ μm or, after frequency doubling in a nonlinear $AgGaS_2$ crystal (thickness 1.5 mm), at $\lambda_{ex} = 2.5$ μm. The major part of the OPCPA output generates femtosecond hard x-ray pulses in a table-top x-ray source [16]. The 5-μm beam is tightly focused onto a 15-μm-thick Cu tape and generates up to 2×10^9 Cu $K\alpha$ photons (photon energy 8 keV) per pulse in the full solid angle. Using a multilayer x-ray optics with a magnification of three (Incoatec), the Cu $K\alpha$ photons are focused onto the sample [spot size 135 μm full width at half maximum (FWHM)]. The x-ray flux on the sample reaches up to $\approx 2 \times 10^7$ photons/s. The x-ray pulse duration is 120 fs.

The optical pump beam is focused onto the sample with a spot size of 420 μm (FWHM), and the angle between the pump and the x-ray beam is around 10°. The optical penetration depths of the pump pulses are approximately 60 and 250 nm at $\lambda_{ex} = 2.5$ and 5 μm, respectively, substantially larger than the 45-nm sample thickness and the 17-nm penetration depth at $\lambda_{ex} = 0.8$ μm [17]. A mechanical chopper in the pump beam (frequency 500 Hz) serves for subsequent measurement of the x-ray response with and without excitation at the same delay time.

Pump-probe traces for different excitation wavelengths, pump fluences, and crystal orientations are summarized in Figs. 1(a)–1(c). The change of diffracted intensity $\Delta I/I_0$ on the (111) Bragg peak is plotted as a function of pump-probe delay ($\Delta I = I - I_0$ with I, I_0 the x-ray intensity detected with and without excitation). Figure 1(a) compares transients for excitation wavelengths of 0.8 and 2.5 μm, Fig. 1(b) shows transients for $\lambda_{ex} = 5$ μm for two different azimuthal orientations ϕ of the Bi film around the (111) symmetry axis [18], and Fig. 1(c) compares transients for different excitation fluences. Apart from the magnitude of the signals, the shape of the transients is very similar. All transients exhibit a fast rise within the 150-fs time resolution of the experiment, an exponential decay with a time constant of 5 ps, superimposed by pronounced oscillations with frequencies around 2.6 THz [see the Fourier spectra in Figs. 1(d)–1(f)], persisting for several picoseconds.

Figure 2(a) summarizes the measured oscillation frequencies (solid circles) and amplitudes $|\Delta I/I_0|$ (open symbols) of the different transients as a function of pump fluence at $\lambda_{ex} = 5$ μm (red symbols) and 2.5 μm (blue symbols). The open diamonds represent the amplitude of the fast decrease after subtraction of the oscillatory part, whereas the open squares give the peak-to-peak amplitude of the oscillations. For $\lambda_{ex} = 5$ μm, below a fluence of 1.9 mJ/cm^2 we do not observe any phonon oscillations above the noise floor of our experiment, in line with results reported by Melnikov *et al.* [10,11]. The fluence dependence of the signal

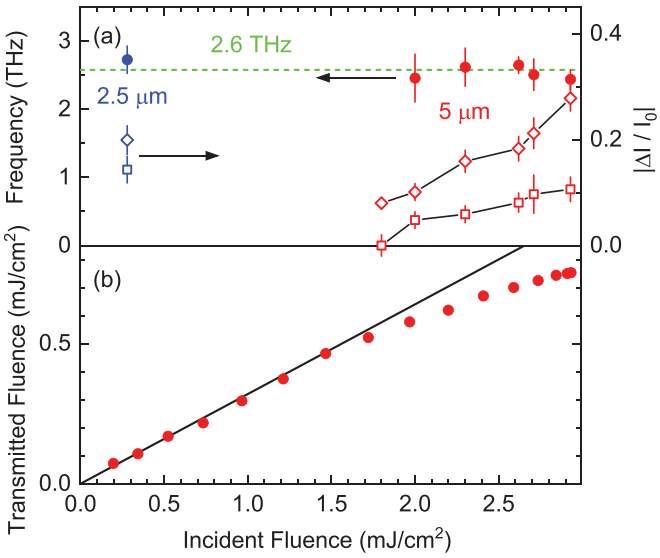

FIG. 2. (a) Left ordinate, solid symbols: Observed phonon frequency as a function of the pump fluence for pump wavelengths of $\lambda_{ex} = 2.5$ μm (blue) and $\lambda_{ex} = 5$ μm (red). Right ordinate, open symbols: Signal amplitudes of the fast intensity decrease (diamonds) and the phonon oscillations (squares). (b) Red circles: Fluence transmitted through the sample as a function of the incident fluence at $\lambda_{ex} = 5$ μm. The black line shows the expected values for linear transmission.

amplitude (red diamonds) shows a pronounced nonlinear increase, whereas the oscillation frequency (green dashed line at 2.6 THz) is practically fluence independent. This observation is in strong contrast to femtosecond diffraction experiments at $\lambda_{ex} = 0.8$ μm showing a linear behavior of $\Delta I/I_0$ of the (111) Bragg reflection as a function of pump fluence and a decrease of the frequency for increasing fluence [6].

In a complementary experiment, the nonlinear transmission of the 5-μm pump pulses through the Bi sample was measured in a geometry identical to the pump-probe studies. The results shown in Fig. 2(b) (red symbols) display enhanced absorption at fluences $F > 1.5$ mJ/cm^2. The enhanced absorption sets in at a fluence similar to the value at which phonon oscillations are observed in the data shown in Fig. 2(a) [27].

THz-pump–THz-probe experiments were performed with single-cycle THz pulses at a center frequency of 1.3 THz and a pump electric-field amplitude of 700 kV/cm [18,28]. The THz pump-probe trace in Fig. 1(g) displays a transmission decrease, which rises within the time resolution of some 0.5 ps and decays with a time constant of ≈5 ps (solid line: numerical fit), similar to the decay of the x-ray transients. The maximum signal amplitudes show a sixfold symmetry as a function of the azimuthal sample orientation ϕ [Fig. 3(d)]. The amplitude of the anisotropic contribution is ten times smaller than the isotropic contribution.

The x-ray data for excitation at $\lambda_{ex} = 2.5$ μm [Fig. 1(a)] display surprisingly strong changes of diffracted intensity for a very low pump fluence of $F = 0.28$ mJ/cm^2, which is in the *perturbative* limit of light-matter interaction. Here, electron-hole pairs are generated by quasiresonant excitation via the direct energy gap at the T point in k space. Calculations of

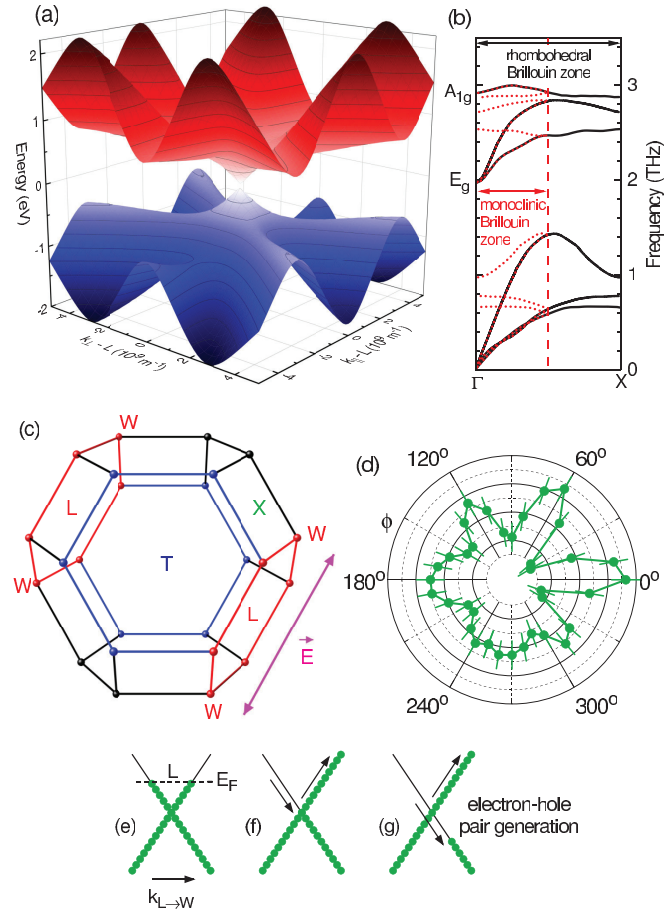

FIG. 3. (a) Calculated electronic band structure of Bi using the density functional theory (DFT) code FLEUR [13,29] around an L point in the Brillouin zone [red hexagon in (c)]. Blue surface: uppermost valence band; red surface: lowermost conduction band. $k_\perp$ is along the connecting line W-L-W and $k_\parallel$ along U-L-U. (b) Black solid lines: Calculated phonon band structure (Fig. 3 of Ref. [30]). In the corresponding monoclinic space group $C2/m$ with four Bi atoms in the unit cell, phonons at X in the rhombohedral space group $R\bar{3}m$ are backfolded to Γ in $C2/m$ (red dotted lines). (c) For a polarization (magenta arrow) parallel to the W-L-W line of an L hexagon the electron-hole-pair generation rate is maximal for this particular L valley, thereby breaking the threefold symmetry of Bi. (d) Azimuthal dependence of the THz-pump–THz-probe signal amplitude. The radial scale for $|\Delta T/T_0|$ is from 0.091 to 0.098. (e)–(g) Schematic electron distributions around the L points for different phases of the vector potential A: (e) at $A = 0$, (f) at $A = E_F/(e\,v_F)$, and (g) for $A > E_F/(e\,v_F)$, which corresponds to (coherently reversible) electron-hole pair generation.

the band structure show that this energy gap depends most sensibly on elongations of Bi atoms along the coordinate of the A_{1g} phonon [18]. In other words, there is a very strong deformation potential coupling of the interband excitation to the A_{1g} phonon, thus enabling a strong coherent phonon excitation even for a very low pump fluence.

At $\lambda_{ex} = 5$ μm, the pump electric field has a peak value on the order of 2 MV/cm resulting in a *nonperturbative* light-matter interaction. In this limit higher-order carrier generation mechanisms occur *in addition* to one-photon absorption and

the different orders *cannot* be disentangled. The electronic band structure around an L point is shown in Fig. 3(a) [13,29], where the carrier energies in the highest valence band and in the lowest conduction band are plotted as functions of $k_\perp$ (along the W-L-W direction) and $k_\parallel$ (along the U-L-U direction). The Brillouin zone and the direction of the (transverse) pump electric field are illustrated in Fig. 3(c). The conelike structure of the highest valence and the lowest conduction band around the L point strongly resembles the band structure of graphene around its K or K' points [31].

The interaction of the pump electric field with carriers around the L point is similar to nonperturbative electron-hole generation in graphene [31–33]. The oscillating pump field drives electrons and/or holes periodically in the field direction in k space. The oscillation amplitude of the carriers is determined by the vector potential, the time integral of the electric field [18]. Carriers far away from the L point perform mainly intraband motions, while carriers close to the L points undergo both intra- and interband motions, illustrated by the yellow double arrows in Fig. S1(b) of the Supplemental Material [18].

In Figs. 3(e)–3(g) we sketch electron distributions around an L point for different phases of the driving vector potential. In equilibrium ($A = 0$ [Fig. 3(e)]) the valence band around the L point is fully occupied, the conduction band up to the Fermi energy E_F. For $A = E_F/(e\,v_F)$ one has the situation in Fig. 3(f) and for the even higher A in our experiments [Fig. 3(g)] one generates additional electron-hole pairs ($v_F = 7.6 \times 10^5$ m/s, with the Fermi velocity determined by the slope of the cone at L). This picture is fully supported by the THz results, which are very close to the nonlinear THz response of graphene [33] and, in particular, show a sixfold azimuthal amplitude dependence for nonperturbative carrier generation at the L points [Fig. 3(d)].

Without scattering processes, i.e., for fully coherent carrier dynamics, the oscillating vector potential A would induce a periodic occurrence and disappearance of electron-hole pairs. In the presence of scattering, however, holes will scatter to the T points where the valence band maxima are located. This process results in decoherence and thus in the irreversible generation of holes at T and electrons at L points.

In our experimental geometry, the driving pump field lies predominantly in the basal plane perpendicular to the [111] direction in real space. As illustrated in Fig. 3(c), for a given direction of the electric field in the sample, the six different interfacial hexagons around the six L points of Bi are not equivalent. Their respective connecting lines, the W-L-W [$k_\perp$-L directions in Fig. 3(a)] form a hexagonal star in the basal plane of the Bi crystal [34]. Thus, for any electric-field direction in the basal plane, carrier generation leads to unequally populated L valleys. For the geometry in Fig. 3(c), there is a predominant population of the red hexagons, while for the other L valleys (black hexagons) the Fermi velocity $v_F(\mathbf{k})$ in the k direction parallel to the driving electric field is much smaller, resulting in an essentially vanishing carrier generation. This also explains the different signal amplitudes for different azimuthal directions ϕ of the electric field [Fig. 1(b)], again in line with the THz results [Fig. 3(d)]. Furthermore, it also shows that the excitation conditions are above the $\chi^{(3)}$ limit, since $\chi^{(3)}$ predicts results independent of ϕ [35].

The asymmetry in L-valley populations reduces the space group of the excited Bi lattice from the original $R\bar{3}m$ to the monoclinic $C2/m$ subgroup (point group $2/m$) with four Bi atoms in its primitive unit cell. In k space, one of the original X points is backfolded to the Γ point of the monoclinic subgroup [18]. As an important consequence, phonon states located at this X point [Fig. 3(b)] in the original space group [30] are now at the Γ point, making them fully accessible for displacive excitation.

Our experimental findings for excitation at $\lambda_{ex} = 5$ μm support this physical picture directly: We observe (i) an increase in carrier generation [Fig. 2(a)], in line with the condition $A > E_F/(e\,v_F)$. This leads (ii) to nonlinear absorption [Fig. 2(b)], as also found in the THz range, and the nonlinear fluence dependence of the x-ray intensity changes $\Delta I/I_0$. (iii) The frequency of the observed phonons is lower than that of the A_{1g} phonon at the Γ point of Bi in $R\bar{3}m$ symmetry and independent from the excitation fluence up to $F = 3$ mJ/cm^2. In contrast, 800 nm excitation yields a linear fluence dependence of $\Delta I/I_0$ and a decrease of the frequency for higher fluences [6]. The photoinduced asymmetry of electron populations in differently oriented L valleys allows now for displacive excitation of coherent zone-boundary phonons (formerly at X in the rhombohedral space group), which are at the Γ point in the excited Bi lattice of $C2/m$ symmetry [18]. Excitation with 5-μm pulses generates predominantly phonons backfolded from X, whereas 800-nm and 2.5-μm pulses generate predominantly A_{1g} phonons at Γ.

In conclusion, different quantum pathways of coherent optical phonon excitation in Bi have been observed after midinfrared optical excitation. Field-driven carrier generation at $\lambda_{ex} = 5$ μm results in a reduction of the symmetry of the unexcited crystal lattice and a backfolding of optical phonon states to the Γ point, making them accessible to displacive excitation. The latter mechanism results in coherent lattice dynamics along different phonon coordinates and not just along the A_{1g} phonon.

Funding by the Deutsche Forschungsgemeinschaft (DFG, German Research Foundation) via the Grant No. WO 558/14-1 to M.W. and through projects B04 and C01 of the Collaborative Research Center SFB 1242 "Nonequilibrium dynamics of condensed matter in the time domain" (Project No. 278162697) is appreciated.

[1] K. Sokolowski-Tinten, C. Blome, J. Blums, A. Cavalleri, C. Dietrich, A. Tarasevitch, I. Uschmann, E. Förster, M. Kammler, M. Horn-von Hoegen, and D. von der Linde, Femtosecond x-ray measurement of coherent lattice vibrations near the Lindemann stability limit, Nature (London) **422**, 287 (2003).

[2] D. M. Fritz, D. A. Reis, B. Adams, R. A. Akre, J. Arthur, C. Blome, P. H. Bucksbaum, A. L. Cavalieri, S. Engemann, S. Fahy, R. W. Falcone, P. H. Fuoss, K. J. Gaffney, M. J. George, J. Hajdu, M. P. Hertlein, P. B. Hillyard, M. Horn-von Hoegen, M. Kammler, J. Kaspar *et al.*, Ultrafast bond softening in bismuth:

Mapping a solid's interatomic potential with x-rays, Science **315**, 633 (2007).

[3] S. L. Johnson, P. Beaud, C. J. Milne, F. S. Krasniqi, E. S. Zijlstra, M. E. Garcia, M. Kaiser, D. Grolimund, R. Abela, and G. Ingold, Nanoscale Depth-Resolved Coherent Femtosecond Motion in Laser-Excited Bismuth, Phys. Rev. Lett. **100**, 155501 (2008).

[4] S. L. Johnson, P. Beaud, E. Vorobeva, C. J. Milne, É. D. Murray, S. Fahy, and G. Ingold, Directly Observing Squeezed Phonon States with Femtosecond X-Ray Diffraction, Phys. Rev. Lett. **102**, 175503 (2009).

[5] S. L. Johnson, P. Beaud, E. Vorobeva, C. J. Milne, É. D. Murray, S. Fahy, and G. Ingold, Non-equilibrium phonon dynamics studied by grazing-incidence femtosecond x-ray crystallography, Acta Crystallogr, Sect. A **66**, 157 (2010).

[6] W. Lu, M. Nicoul, U. Shymanovich, A. Tarasevitch, M. Kammler, M. Horn von Hoegen, D. von der Linde, and K. Sokolowski-Tinten, Extreme phonon softening in laser-excited bismuth—towards an inverse Peierls-transition, MRS Online Proc. Libr. **1230**, 305 (2009).

[7] H. J. Zeiger, J. Vidal, T. K. Cheng, E. P. Ippen, G. Dresselhaus, and M. S. Dresselhaus, Theory for displacive excitation of coherent phonons, Phys. Rev. B **45**, 768 (1992).

[8] M. Hase, M. Kitajima, S. I. Nakashima, and K. Mizoguchi, Dynamics of Coherent Anharmonic Phonons in Bismuth Using High Density Photoexcitation, Phys. Rev. Lett. **88**, 067401 (2002).

[9] É. D. Murray, D. M. Fritz, J. K. Wahlstrand, S. Fahy, and D. A. Reis, Effect of lattice anharmonicity on high-amplitude phonon dynamics in photoexcited bismuth, Phys. Rev. B **72**, 060301(R) (2005).

[10] A. A. Melnikov, O. V. Misochko, and S. V. Chekalin, Generation of coherent phonons in bismuth by ultrashort laser pulses in the visible and NIR: Displacive versus impulsive excitation mechanism, Phys. Lett. A **375**, 2017 (2011).

[11] A. A. Melnikov, O. V. Misochko, and S. V. Chekalin, Ultrafast electronic dynamics in laser-excited crystalline bismuth, J. Appl. Phys. **114**, 033502 (2013).

[12] I. Timrov, T. Kampfrath, J. Faure, N. Vast, C. R. Ast, C. Frischkorn, M. Wolf, P. Gava, and L. Perfetti, Thermalization of photoexcited carriers in bismuth investigated by time-resolved terahertz spectroscopy and *ab initio* calculations, Phys. Rev. B **85**, 155139 (2012).

[13] I. Aguilera, C. Friedrich, and S. Blügel, Electronic phase transitions of bismuth under strain from relativistic self-consistent *GW* calculations, Phys. Rev. B **91**, 125129 (2015).

[14] M. Kammler and M. Horn-von Hoegen, Low energy electron diffraction of epitaxial growth of bismuth on Si(1 1 1), Surf. Sci. **576**, 56 (2005).

[15] L. von Grafenstein, M. Bock, D. Ueberschaer, E. Escoto, A. Koç, K. Zawilski, P. Schunemann, U. Griebner, and T. Elsaesser, Multi-millijoule, few-cycle 5 μm OPCPA at 1 kHz repetition rate, Opt. Lett. **45**, 5998 (2020).

[16] A. Koç, C. Hauf, M. Woerner, L. von Grafenstein, D. Ueberschaer, M. Bock, U. Griebner, and T. Elsaesser, Compact high-flux hard x-ray source driven by femtosecond mid-infrared pulses at a 1 kHz repetition rate, Opt. Lett. **46**, 210 (2021).

[17] A. P. Lenham, D. M. Treherne, and R. J. Metcalfe, Optical properties of antimony and bismuth crystals, J. Opt. Soc. Am. **55**, 1072 (1965).

[18] See Supplemental Material at http://link.aps.org/supplemental/10.1103/PhysRevB.107.L180303 for additional details on the mechanism of displacive excitation of phonons, on perturbative and nonperturbative light-matter interactions, on symmetry aspects, on the THz experiments, and on the phonon assignments, which includes Refs. [19–26].

[19] M. Bargheer, N. Zhavoronkov, J. C. Woo, D. S. Kim, M. Woerner, and T. Elsaesser, Excitation mechanisms of coherent phonons unravelled by femtosecond x-ray diffraction, Phys. Status Solidi B **243**, 2389 (2006).

[20] *International Tables for Crystallography*, edited by T. Hahn, 5th ed. (Springer, Dordrecht, 2005), Vol. A.

[21] T. Kuhn, Density matrix theory of coherent ultrafast dynamics, in *Theory of Transport Properties of Semiconductor Nanostructures*, edited by E. Schöll (Chapman & Hall, London, 1998), pp. 173–214.

[22] W. Kuehn, P. Gaal, K. Reimann, M. Woerner, T. Elsaesser, and R. Hey, THz-induced interband tunneling of electrons in GaAs, Phys. Rev. B **82**, 075204 (2010).

[23] O. Schubert, M. Hohenleutner, F. Langer, B. Urbanek, C. Lange, U. Huttner, D. Golde, T. Meier, M. Kira, S. W. Koch, and R. Huber, Sub-cycle control of terahertz high-harmonic generation by dynamical Bloch oscillations, Nat. Photonics **8**, 119 (2014).

[24] T. Elsaesser, K. Reimann, and M. Woerner, *Concepts and Applications of Nonlinear Terahertz Spectroscopy* (Morgan & Claypool, San Rafael, CA, 2019).

[25] R. M. Brugger, R. B. Bennion, and T. G. Worlton, The crystal structure of bismuth-II at 26 kbar, Phys. Lett. A **24**, 714 (1967).

[26] L. G. Akselrud, M. Hanfland, and U. Schwarz, Refinement of the crystal structure of Bi-II, at 2.54 GPa, Z. Kristallogr. - New Cryst. Struct. **218**, 415 (2003).

[27] Under our conditions nonlinear absorption in the silicon substrate is negligible—see X. Gai, Y. Yu, B. Kuyken, P. Ma, S. J. Madden, J. V. Campenhout, P. Verheyen, G. Roelkens, R. Baets, and B. Luther-Davies, Nonlinear absorption and refraction in crystalline silicon in the mid-infrared, Laser Photonics Rev. **7**, 1054 (2013).

[28] A. Ghalgaoui, L.-M. Koll, B. Schütte, B. P. Fingerhut, K. Reimann, M. Woerner, and T. Elsaesser, Field-induced tunneling ionization and terahertz-driven electron dynamics in liquid water, J. Phys. Chem. Lett. **11**, 7717 (2020).

[29] D. Wortmann, G. Michalicek, R. Hilgers, A. Neukirchen, H. Janssen, U. Grytsiuk, J. Broeder, and C.-R. Gerhorst, DFT code FLEUR, http://www.flapw.de.

[30] L. E. Díaz-Sánchez, A. H. Romero, and X. Gonze, Phonon band structure and interatomic force constants for bismuth: Crucial role of spin-orbit interaction, Phys. Rev. B **76**, 104302 (2007).

[31] M. Woerner, T. Elsaesser, and K. Reimann, Nonlinear terahertz spectroscopy on multilayer graphene, in *Optical Properties of Graphene*, edited by R. Binder (World Scientific, Singapore, 2017), pp. 269–293.

[32] K. L. Ishikawa, Nonlinear optical response of graphene in time domain, Phys. Rev. B **82**, 201402(R) (2010).

[33] P. Bowlan, E. Martinez-Moreno, K. Reimann, T. Elsaesser, and M. Woerner, Ultrafast terahertz response of multilayer graphene in the nonperturbative regime, Phys. Rev. B **89**, 041408(R) (2014).

[34] P. Zhou, C. Streubühr, M. Ligges, T. Brazda, T. Payer, F. Meyer zu Heringdorf, M. Horn-von Hoegen, and D. von der Linde, Transient anisotropy in the electron diffraction of femtosecond laser-excited bismuth, New J. Phys. **14**, 103031 (2012).

[35] S. V. Gallego, J. Etxebarria, L. Elcoro, E. S. Tasci, and J. M. Perez-Matoa, Automatic calculation of symmetry-adapted tensors in magnetic and non-magnetic materials: a new tool of the Bilbao Crystallographic Server, Acta Crystallogr., Sect. A **75**, 438 (2019).